Metastable speeds in the fractional Allen-Cahn equation

F. Achleitner, C. Kuehn, J.M. Melenk, A. Rieder

Most recent ASC Reports

12/2020   A. Haberl, D. Praetorius, S. Schimanko, and M. Vohralik
          Convergence and quasi-optimal cost of adaptive algorithms for nonlinear ope-
          rators including iterative linearization and algebraic solver

11/2020   L. Banjai, J.M. Melenk, and C. Schwab
          hp-FEM for reaction-diffusion equations
          II. Robust exponential convergence for multiple length scales in corner domains

10/2020   G. Gantner and D. Praetorius
          Adaptive BEM for elliptic PDE systems,
          Part I: Abstract framework for weakly-singular integral equations

09/2020   C. Helmer and A. Jüngel
          Analysis of Maxwell-Stefan systems for heat conducting fluid mixtures

08/2020   L. Mascotto, J.M. Melenk, I. Perugia, A. Rieder
          FEM-BEM mortar coupling for the Helmholtz problem in three dimensions

07/2020   R. Becker, M. Innerberger, and D. Praetorius
          Optimal convergence rates for goal-oriented FEM with quadratic goal functional

06/2020   A. Rieder, F.-J. Sayas, J.M. Melenk
          Runge-Kutta approximation for C_0-semigroups in the graph norm with applica-
          tions to time domain boundary integral equations

05/2020   A. Arnold, C. Schmeiser, and B. Signorello
          Propagator norm and sharp decay estimates for Fokker-Planck equations with
          linear drift

04/2020   G. Gantner, A. Haberl, D. Praetorius, and S. Schimanko
          Rate optimality of adaptive finite element methods with respect to the overall
          computational costs

03/2020   M. Faustmann, J.M. Melenk, M. Parvizi
          On the stability of Scott-Zhang type operators and application to multilevel
          preconditioning in fractional diffusion

Metastable Speeds in the Fractional Allen-Cahn Equation

Franz Achleitner[*], Christian Kuehn[†], Jens M. Melenk[*] and Alexander Rieder[‡]

June 8, 2020

Abstract

We study numerically the one-dimensional Allen-Cahn equation with the spectral fractional Laplacian $(-\Delta)^{\alpha/2}$ on intervals with homogeneous Neumann boundary conditions. In particular, we are interested in the speed of sharp interfaces approaching and annihilating each other. This process is known to be exponentially slow in the case of the classical Laplacian. Here we investigate how the width and speed of the interfaces change if we vary the exponent α of the fractional Laplacian. For the associated model on the real-line we derive asymptotic formulas for the interface speed and time–to–collision in terms of α and a scaling parameter ε. We use a numerical approach via a finite-element method based upon extending the fractional Laplacian to a cylinder in the upper-half plane, and compute the interface speed, time–to–collapse and interface width for $\alpha \in (0.2, 2]$. A comparison shows that the asymptotic formulas for the interface speed and time–to–collision give a good approximation for large intervals.

1 Introduction

In this work we study the fractional Allen-Cahn equation

$$\partial_t u = -\varepsilon^\alpha (-\Delta)^{\alpha/2} u + u(1 - u^2) =: -\varepsilon^\alpha (-\Delta)^{\alpha/2} u - f(u), \tag{1}$$

for $u = u(x,t)$, where $(x,t) \in \Omega \times [0,T]$, $\Omega := [-L, L]$ is the spatial domain for $L > 0$, $-(-\Delta)^{\alpha/2}$ is the fractional Laplacian for $\alpha \in (0, 2]$, and $0 < \varepsilon \ll 1$ is a small parameter. We assume homogeneous Neumann boundary conditions and an initial condition

$$\partial_x u(-L, t) = 0 = \partial_x u(L, t), \qquad u(x, 0) = u_0(x),$$

for some given initial datum $u_0 = u_0(x)$. We consider the *spectral* fractional Laplacian, which is defined as

$$(-\Delta)^{\alpha/2} u := \sum_{n=0}^{\infty} \lambda_n^{\alpha/2} (u, \varphi_n)_{L^2(\Omega)} \, \varphi_n$$

---

[*]Technische Universität Wien, Institute for Analysis and Scientific Computing, Wiedner Hauptstrae 8-10 1040 Wien, Austria

[†]Technical University of Munich (TUM), Faculty of Mathematics, 85748 Garching bei München, Germany

[‡]University of Vienna, Faculty of Mathematics, Oskar-Morgenstern-Platz 1, 1090 Wien, Austria

where (λ_n, φ_n) are the eigenvalues and eigenfunctions of the Laplacian with homogeneous Neumann boundary conditions scaled such that $\|\varphi_n\|_{L^2(\Omega)} = 1$. Other possible definitions for fractional Laplacians on bounded domains with Neumann-type boundary conditions are discussed and compared in [13, §7] and [15, §6].

The potential F associated to $f(u) = u(u^2 - 1)$ via $F'(u) = f(u)$ is given by

$$F(u) := \frac{1}{4}u^4 - \frac{1}{2}u^2 \, .$$

There are three homogeneous steady states for (1) given by $u_* = -1, 0, 1$. Using the linearized problem

$$\partial_t U = \underbrace{\left[-\varepsilon^\alpha (-\Delta)^{\alpha/2} - D_u f(u_*) \right]}_{:=L(u_*)} U, \qquad U = U(x, t),$$

one easily checks that $u_* = \pm 1$ are locally asymptotically stable since the spectrum of $L(u_*)$ is contained in $\{z \in \mathbb{C} : \operatorname{Re}(z) < 0\}$. The state $u_* = 0$ is unstable. Indeed, one can also view $u_* = \pm 1$ as global minima and $u_* = 0$ as a local maximum of the potential F.

For the case of $\alpha = 2$, so that $-(-\Delta)^{\alpha/2} = \Delta$, even more global dynamics of (1) is well understood; see Section 2.1 for a more detailed technical review. Here we just emphasize that the Allen-Cahn equation (1) can exhibit metastability as shown in Figure 1.
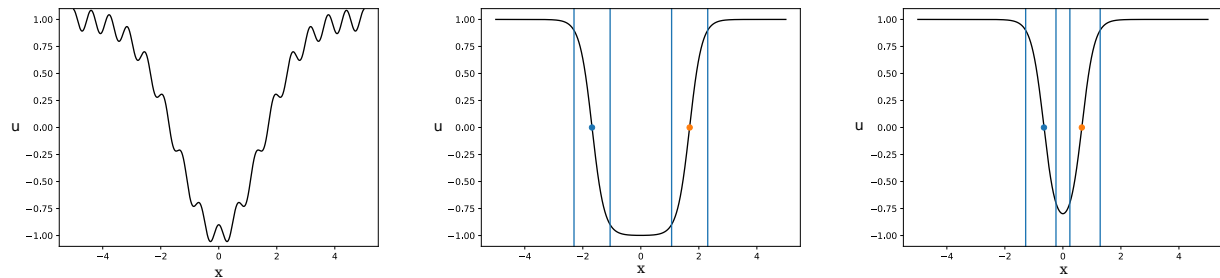
(a) solution at time $t = 0$.   (b) solution at time $t = 1771$.   (c) solution at time $t = 177216$.

Figure 1: Evolution of solution for the classical Allen-Cahn equation (1) for (11) with $L = 5$, $\varepsilon = 0.3$ and $\alpha = 2$.

We observe that suitable initial conditions u_0 get attracted very quickly to solutions composed of multiple, say n, very sharp interfaces. Each interface is known to have width $\mathcal{O}(\varepsilon)$ for $\alpha = 2$; see Section 2.1. For a long time, this n-interface solution appears to be stationary, but it evolves on an exponentially long time scale $\mathcal{O}(e^{K/\varepsilon})$ for some constant $K > 0$; see again Section 2.1 for details. On this exponentially long time scale the interfaces move towards each other and then annihilate; see Figure 1. This effect is the essence of *metastable behavior*, i.e., apparent stationarity on extremely long, yet still transient, time scales.

In this work, we are interested in the influence of the parameter α on metastable interface motion. It is natural to ask how the order of the fractional Laplacian influences the interface speed as well as the interface width. For $\alpha = 2$, these effects have been quantified, see, e.g., [9]. However, for $\alpha = (0, 2)$ a precise quantification has not been carried out yet.

However, this problem has been studied for (1) with the fractional Laplacian on the real line. For $\alpha \in (1, 2)$ the dependence of the interface speed has been quantified by heuristic

arguments and verified numerically via a pseudo-spectral method [25]. Moreover, equation (1) with periodic potential F and external forcing on the real line has been studied as a model in crystal dislocation dynamics, see [14, 11, 12, 27, 28, 29]. They characterize the long-time behavior of solutions which includes metastable scenarios and give rigorous proofs.

It is not obvious if these results carry over to the fractional Allen-Cahn equation (1) with homogeneous Neumann boundary conditions. For example, the fractional Laplacian on the real line is uniquely defined, e.g. see [19], whereas on bounded intervals several distinct definitions exist, see [30, 15, 13, 21]. However our numerical studies of the interface motion for (1) with homogeneous Neumann boundary conditions indicate that the interface speed is governed by the same asymptotic dependence on ε and α. Additionally, we characterize the dependence of the interface width on these parameters. In particular, our main observations are:

(R1) *Interface speed:* For $\alpha \in (0.5, 2)$, the magnitude of the interface speed in case of two interfaces is approximately

$$|s(\varepsilon, \alpha)| \approx \varepsilon^{1+\alpha} \, \frac{4}{\alpha} \frac{2^\alpha \Gamma((1+\alpha)/2)}{\sqrt{\pi}|\Gamma(-\alpha/2)|} \, \gamma \, \frac{1}{|x_1 - x_2|^\alpha} \, . \tag{2}$$

where x_1 and x_2 are the centers of the interfaces and $\gamma := (\int_{\mathbb{R}} (v'(x))^2 \mathrm{d}x)^{-1}$ is the inverse of the semi-norm of a basic layer solution v of (9)–(10).

(R2) *Interface width:* For $\alpha \in (0.2, 2)$, the interface width is approximately

$$w(\varepsilon, \alpha) = b(\alpha)\varepsilon^{\kappa_1 \alpha^{-1} + \kappa_2} \, , \tag{3}$$

where we numerically estimated $\kappa_1 \approx -0.168298$ and $\kappa_2 \approx 1.11709$. We note that the numerically estimates suggest the *conjectures* $\kappa_1 = 1/6$ and $\kappa_2 = 10/9$.

The paper is structured as follows: In Section 2, we briefly review analytical results for the Allen-Cahn equation involving the Laplacian ($\alpha = 2$) with homogeneous Neumann boundary conditions and the fractional Laplacian ($\alpha \in (0, 2)$) on the real line, respectively. In Section 3, we describe the numerical setup used to simulate (1) for $\alpha \in (0, 2]$. Moreover, we compare our numerical method with a spectral method in §3.3. The main results are presented and discussed in Section 4. A brief summary and an outlook to future open problems can be found in Section 5.

2 Asymptotic analysis

2.1 The Classical Case

In this section, we briefly review the known results for metastability of the classical Allen-Cahn equation

$$\partial_t u = \varepsilon^2 \partial_{xx} u + u(1 - u^2), \tag{4}$$

with Neumann boundary conditions posed on the interval $[0, 1]$ as studied by several authors; here we mainly follow [9]. Note that considering the interval $[0, 1]$ is equivalent to picking $[-L, L]$ up to shifting and scaling the x-coordinate. A key auxiliary tool to construct n-interface

solutions is to first construct a single layer. This requires the solution of the auxiliary two-point boundary value problem

$$\varepsilon^2 \frac{\mathrm{d}^2\phi}{\mathrm{d}x^2} = \phi(1 - \phi^2), \qquad \phi(-\ell/2) = 0 = \phi(\ell/2). \tag{5}$$

For $\varepsilon > 0$ sufficiently small, it can be proven that (5) has a unique solution $\phi(x, \ell)$ for each given $\ell > 0$, which is positive for $|x| < \ell/2$. The shape of $\phi(x, \ell)$ corresponds to a spike centered at $x = 0$, i.e., an interior layer solution in the terminology of multiscale analysis [18]. The width of this spike is $\mathcal{O}(\varepsilon)$ and it can also be interpreted as a homoclinic orbit in (ϕ, ϕ')-coordinates to $(0, 0)$. Next, one wants to construct an interface (layer) with location $h = h(t)$ for (4). Consider a monotone function

$$\xi \in C^\infty(\mathbb{R}, [0, 1]), \qquad \xi(x) = \begin{cases} 0 & \text{for } x \leq -1, \\ 1 & \text{for } x \geq 1, \end{cases}$$

and define the *approximate metastable interface*, $u^h = u^h(x)$ for some $0 < h < 1$ by

$$u^h(x) := -\left[1 + \xi\left(\frac{x-h}{\varepsilon}\right)\right]\phi(x, 2h) + \xi\left(\frac{x-h}{\varepsilon}\right)\phi(x-1, 2-2h) \tag{6}$$

so that $u^h(0) < 0$, $u^h(h) = 0$, $u^h(1) > 0$, and the width of the interface is $\mathcal{O}(\varepsilon)$. Obviously one can construct an approximate n-interface solution by a similar procedure. Since any n-interface solution has n natural coordinates given by the positions h of each interface, one can define an n-dimensional manifold $\mathcal{M}$ in $H^1([0, 1])$ parametrized by the positions. It is shown in [9] that this manifold is locally attracting for large classes of initial data for (4). Once the solution is close to the approximately invariant manifold $\mathcal{M}$, there exists an ODE describing the motion of the positions h on $\mathcal{M}$. It turns out that all interface positions move at equal asymptotic speed in a generic setting away from any annihilation events. Their speed in this regime can be determined by just looking at one interface. It is highly non-trivial to prove that the ODE for its position is given by

$$h' = K_0\varepsilon\left[q\left(\frac{\varepsilon}{2h}\right) - q\left(\frac{\varepsilon}{2 - 2h}\right)\right] + R_1, \qquad q(r) := F(\phi(0, \ell)), \ r := \varepsilon/\ell, \tag{7}$$

where $K_0 > 0$ is a computable order $\mathcal{O}(1)$ constant, and R_1 turns out to be a negligible remainder term [9]. Metastability arises because one can also prove that

$$q(r) = K_1 e^{-K_2\ell/\varepsilon} + R_2,$$

for constants $K_{1,2} > 0$ and R_2 turns out to be another higher-order terms irrelevant for computing the leading-order of the vector field in (7), i.e., the local interface speed is exponentially small for $\alpha = 2$.

2.2 Analysis of fractional Allen-Cahn equations

For $\alpha \in (0, 2)$, the results for the classical case lead to the following questions:

(Q1) Does the metastable interface speed $s = s(\varepsilon, \alpha)$ change? If so, what is the graph of $s(\varepsilon, \alpha)$ as a function of α and/or ε?

(Q2) Does the interface width $w = w(\varepsilon, \alpha)$ change? If so, what is the graph of $w(\varepsilon, \alpha)$ as a function of α and/or ε?

The questions (Q1)-(Q2) are our main focus as they provide immediate information on the relevant dynamical behavior.

We discuss the ambitious task to extend the results by Carr and Pego in the Section 5. Next, we will present the analysis of a fractional Allen-Cahn equation on $\mathbb{R}$, which provides approximations for the interface speed and time–to–collapse. In Section 4 we show by numerical simulations that these formulas also give a good approximation for our model on a bounded interval.

2.2.1 Analysis of fractional Allen-Cahn equations on $\mathbb{R}$

Equation (1) with periodic potential F and external forcing on the real line $x \in \mathbb{R}$ models the dynamics of crystal dislocations, see [14, 11, 12, 27, 28, 29]. First, the evolution of dislocations given as a superposition of transitions with the same orientation has been studied. It has been shown that these transitions repel each other [14, 11, 12]. Patrizi and Valdinoci [27, 28, 29] considered also dislocations given as a superposition of transitions with arbitrary orientations and studied again the long-time behavior. For example, two transitions of opposite orientation attract each other (if no external force is present), which shows the metastable behavior we are interested in. In general, they study the long-time behavior of well–prepared initial data modeling an arbitrary (but finite) number of transitions with any order of orientations. We report here their results for the equation

$$\partial_t u_\varepsilon = \tfrac{1}{\varepsilon}\Big(-(-\Delta)^{\alpha/2} u_\varepsilon - \tfrac{1}{\varepsilon^\alpha} F'(u_\varepsilon) \Big), \tag{8}$$

on $x \in \mathbb{R}$ with (non-periodic) potential $F(u) = \frac{u^4}{4} - \frac{u^2}{2}$ and superposition of transitions with alternating orientations (and note the minor modifications needed along the way):

Equations (1) and (8) are related via a rescaling of time $t \mapsto t/\varepsilon^{1+\alpha}$.

First, a well–prepared initial datum u_0 is constructed from basic layer solutions of (1) (instead of initial layer solutions): A basic layer solution $v : \mathbb{R} \to [-1, 1]$ is a stationary solution of (1), i.e. it solves

$$-(-\Delta)^{\alpha/2} v - f(v) = 0, \qquad x \in \mathbb{R}, \tag{9}$$

and satisfies

$$v'(x) > 0 \text{ for all } x \in \mathbb{R}, \quad v(-\infty) = -1, \quad v(0) = 0, \quad v(+\infty) = 1. \tag{10}$$

Here, with a slight abuse of notation $-(-\Delta)^{\alpha/2}$ denotes the fractional Laplacian acting on functions on the real line. Note that the fractional Laplacian given on the real line is equivalent to a singular integral representation, see [8, 19]. The existence and uniqueness (due to $v(0) = 0$) of a basic layer solution has been proved in [7, Thm. 2.4].

Then, a well–prepared initial datum u_0 is constructed from shifted basic layer solutions v of alternating orientation. For example, we study the evolution of a transition layer given by

$$u_\varepsilon^0(x) := v\left(\frac{x - x_1^0}{\varepsilon} \right) + v\left(-\frac{x - x_2^0}{\varepsilon} \right) + 1 \tag{11}$$

5

for some $x_2^0 < x_1^0$. More generally, we study the evolution of an initial datum u_ε^0 given by

$$u_\varepsilon^0(x) := \sum_{i=1}^{2K} v_{\varepsilon,i}^0(x) + 1 \tag{12}$$

where $K \in \mathbb{N}$, $v_{\varepsilon,i}^0(x) = v\left(\zeta_i \frac{x-x_i^0}{\varepsilon}\right)$ with $x_{2K}^0 < x_{2K-1}^0 < \ldots < x_2^0 < x_1^0$ and

$$\zeta_i = \begin{cases} +1 & \text{if } i \text{ is odd}, \\ -1 & \text{if } i \text{ is even}, \end{cases} \qquad i \in \{1, 2, \ldots, 2K\}.$$

It can be shown that, for sufficiently small $\varepsilon > 0$, the solution $u_\varepsilon(x,t)$ of (8) with initial datum u_ε^0 is approximately of the form

$$u_\varepsilon(x,t) \approx \sum_{i=1}^{2K} v\left(\zeta_i \frac{x-x_i(t)}{\varepsilon}\right) + 1, \tag{13}$$

where the functions $x_i(t)$ satisfy approximately (i.e., up to higher order terms in ε) a system of ODEs

$$\begin{cases} \frac{\mathrm{d}x_i}{\mathrm{d}t} = \frac{\varepsilon^{1+\alpha}}{\alpha} 4 \frac{2^\alpha \Gamma((1+\alpha)/2)}{\sqrt{\pi}|\Gamma(-\alpha/2)|} \gamma \sum_{i \neq j} \zeta_i \zeta_j \frac{x_i - x_j}{|x_i - x_j|^{1+\alpha}}, \\ x_i(0) = x_i^0, \end{cases} \tag{14}$$

for $i \in \{1, 2, \ldots, 2K\}$ and $\gamma := \left(\int_{\mathbb{R}} (v'(x))^2 \mathrm{d}x\right)^{-1}$. The centers x_i are initially ordered as $x_{2K}^0 < x_{2K-1}^0 < \ldots < x_2^0 < x_1^0$, then for sufficiently small times $t > 0$ this order will persist for the solution of (14), i.e.

$$x_{2K}(t) < x_{2K-1}(t) < \ldots < x_2(t) < x_1(t). \tag{15}$$

System (14) is well-defined until the first collision at time T_C, which is defined as the time such that (15) holds for all $t \in [0, T_C)$ and

$$\exists i_C \in \{1, 2, \ldots, 2K-1\} : \qquad x_{i_C+1}(T_C) = x_{i_C}(T_C). \tag{16}$$

More precisely, it is proved that the solution u_ε approaches a superposition of sharp transitions with moving centers $x_i(t)$ in the following sense:

Theorem 2.1 (cf. [27, Thm. 1.1]). *Suppose $\alpha \in [1, 2]$. Let*

$$v(t,x) = \sum_{i=1}^{2K} \mathrm{sgn}(\zeta_i(x - x_i(t))) + 1, \tag{17}$$

where sgn *is the sign function and $(x_i(t))_{i=1,\ldots,2K}$ is the solution to (14). Then, for every $\varepsilon > 0$ there exists a unique solution u_ε of (8). Furthermore, as $\varepsilon \to 0^+$, the solution u_ε exhibits the following asymptotic behavior:*

$$\limsup_{\substack{(t',x') \to (t,x) \\ \varepsilon \to 0^+}} u_\varepsilon(t', x') \leq \limsup_{(t',x') \to (t,x)} v(t', x') \tag{18}$$

and

$$\liminf_{\substack{(t',x') \to (t,x) \\ \varepsilon \to 0^+}} u_\varepsilon(t', x') \geq \liminf_{(t',x') \to (t,x)} v(t', x') \tag{19}$$

for any $(t, x) \in [0, T_C) \times \mathbb{R}$.

Sketch of proof. The initial conditions u_ε^0 under consideration take values in $[-1, 1]$. Due to a maximum principle for (8), the corresponding solution u_ε of (8) with initial datum u_ε^0 will again satisfy $-1 \leq u_\varepsilon(t, x) \leq 1$ for all (t, x). We consider (8) with the periodic potential F_{per} such that $F_{per}(u) = F(u)$ for all $u \in [-1, 1]$. Then $F_{per} \in C^{2,\beta}(\mathbb{R})$ is Hölder continuous. Now we can use the result of [27, Thm. 1.1] for the modified problem. However, since $-1 \leq u_\varepsilon(t, x) \leq 1$ for all (t, x), the statement carries over to the original problem unchanged. $\qquad\square$

Remark 2.2.   1. The restriction to $\alpha \in [1, 2]$ seems to be due to technical conditions in the proofs. In case of $\alpha \in (0, 1)$, the assumption $F \in C^{3,\beta}(\mathbb{R})$ for some $\beta > 0$ is needed, see [11].

2. In the studies on crystal dislocation dynamics the stable stationary states are taken to be 0 and 1 compared to -1 and 1 as in our setting. That means, we have to include e.g. an affine transformation $y \mapsto -2y + 1$ which gives an additional multiplicative constant 4.

3. Moreover, we have to include a normalization factor $\frac{2^\alpha \Gamma((1+\alpha)/2)}{\sqrt{\pi} |\Gamma(-\alpha/2)|}$, due to the singular integral representations used in [33, Lemma 5.1] compared with [27, (1.2)].

In case of two initial transitions with opposite orientation the following estimate for the time–to–collision T_C holds

Theorem 2.3 (cf. [27, Thm. 1.2]). *Let $K = 1$. Let $d_0 := x_1^0 - x_2^0 > 0$. Then,*

$$T_C = \frac{C_\alpha d_0^{1+\alpha}}{2(1+\alpha)\gamma} \qquad with \ C_\alpha := 1 / \left(\frac{4}{\alpha} \frac{2^\alpha \Gamma((1+\alpha)/2)}{\sqrt{\pi} |\Gamma(-\alpha/2)|} \right) = \frac{\Gamma(1-\alpha)}{2\sec(\alpha\frac{\pi}{2})} \, . \tag{20}$$

Then, (18) and (19) imply that for any $x \neq x_c$ where $x_c := x_1(T_C) = x_2(T_C)$, we have

$$\lim_{t \to T_C^-} \lim_{\varepsilon \to 0^+} u_\varepsilon(t, x) = 1 \, .$$

That means two dislocations annihilate each other after their collision. However, the limit of $u_\varepsilon(t, x)$ keeps a memory of them, in the sense that u_ε at the point x_c does not approach the state 1 in the limit.

Theorem 2.4 ([27, Thm. 1.4]). *Let $K = 1$. Let u_ε be the solution to (8), then*

$$\liminf_{\substack{t \to T_C^- \\ \varepsilon \to 0^+}} u_\varepsilon(t, x_c) \leq -1 \, . \tag{21}$$

Nonetheless, after some time T_ε – which is only slightly larger than the collision time T_C – the solution u_ε will become small like ε. More precisely,

Theorem 2.5 (cf. [28, Thm. 1.1 & Thm. 1.2]). *Let $K = 1$. Under the assumptions of Theorem 2.1, let u_ε be a solution of (8). Then, there exists $\varepsilon_0 > 0$ such that for all $\varepsilon < \varepsilon_0$ there exist $T_\varepsilon, \rho_\varepsilon > 0$ such that*

$$T_\varepsilon = T_C + o(1), \quad \rho_\varepsilon = o(1) \quad as \ \varepsilon \to 0$$

and

$$1 - u_\varepsilon(T_\varepsilon, x) \leq \rho_\varepsilon \quad for \ all \ x \in \mathbb{R}. \tag{22}$$

Moreover, there exist $\tilde{\varepsilon}_0 > 0$ and $c > 0$ such that for any $\varepsilon < \tilde{\varepsilon}_0$ we have

$$|1 - u_\varepsilon(t, x)| \leq \rho_\varepsilon \exp\left(c \frac{T_\varepsilon - t}{\varepsilon^{1+\alpha}}\right), \quad for \ all \ x \in \mathbb{R} \ and \ t \geq T_\varepsilon. \tag{23}$$

3   Numerical Methods

In recent years the numerical simulations of partial differential equations with fractional space derivatives has attracted a lot of attention. Some references on (various forms of) fractional Allen-Cahn equations in one and multi-dimensional spatial settings are the following: [6, 35, 34, 1, 31, 32, 36, 17, 3, 20, 22, 16].

In order to discretize (1), we consider an alternative formulation of the fractional Laplacian, based on the Caffarelli-Silvestre extension [8], as presented in [33] for the Neumann problem. Consider the solution $\mathcal{U} : \mathbb{R}_+ \times \Omega \times \mathbb{R}_+ \to \mathbb{R}$ to:

$$-\operatorname{div}\left(y^{1-\alpha}\mathcal{U}(t)\right) = 0\,, \qquad\qquad \text{in } \Omega \times \mathbb{R}_+\,,\ \forall t > 0\,, \tag{24a}$$

$$d_\alpha \operatorname{tr}\mathcal{U}_t + \varepsilon^2 \partial_\nu^\alpha \mathcal{U} = -d_\alpha f(\operatorname{tr}\mathcal{U})\,, \qquad \text{in } \Omega \times \{0\} \times \mathbb{R}_+\,, \tag{24b}$$

$$\partial_\nu \mathcal{U}(t) = 0\,, \qquad\qquad \text{on } \partial\Omega \times \mathbb{R}_+,\ \forall t > 0\,, \tag{24c}$$

$$\operatorname{tr}\mathcal{U}(0) = u_0\,, \qquad\qquad \text{in } \Omega. \tag{24d}$$

Here $d_\alpha := 2^{1-\alpha}\Gamma(1-\alpha/2)/\Gamma(\alpha/2)$, ∂_ν denotes the normal derivative with respect to the lateral boundary, tr denotes the trace operator with respect to the artificial variable y at 0 and ∂_ν^α is defined by

$$\partial_\nu^\alpha \mathcal{U} := -\lim_{y\to 0^+} y^{1-\alpha}\partial_y \mathcal{U}(\cdot, y).$$

It can then be proven that if $\mathcal{U}$ solves (24), then $\operatorname{tr}\mathcal{U}$ solves (1).

The discretization is based on an semi-implicit BDF2 discretization of the time variable, and a hp-finite element method to discretize the x and y variables, similar to what was presented in [4] for the linear stationary case and [26] for the linear time-dependent fractional diffusion problem, but which is based on a low order discretization in space. An analogous hp-type method for the linear fractional heat equation, but using different time-stepping and Dirichlet boundary condition was analyzed in detail in [24].

The semi-implicit BDF2 (SBDF2) method for the ODE $u_t = \mathscr{L}u + f(t, u)$ with stiff operator $\mathscr{L}$ is given by

$$u^{n+1} = \frac{4}{3}u^n - \frac{1}{3}u^{n-1} + \frac{2}{3}\Delta t\left[2f(t_n, u^n) - f(t_{n-1}, u^{n-1})\right] + \frac{2}{3}\Delta t\mathscr{L}u^{n+1}.$$

For the discretization in the auxiliary variable y, we fix $\sigma \in (0,1)$ and consider a graded mesh $\mathcal{T}_y := \{y_0, \ldots y_N\}$ with $y_0 := 0$, $y_j := \mathcal{Y}\sigma^{N-j}$. Here $\mathcal{Y} > 0$ is a cutoff parameter. In $\Omega := (-L, L)$, we consider a uniform mesh with size $h > 0$, denoted by $\mathcal{T}_x$. Denoting by $\mathcal{S}^{p,1}(\mathcal{T})$ the space of continuous piecewise polynomials of degree p, on a triangulation $\mathcal{T}$ we solve in each time step for $\mathcal{U}_h^{n+1} \in \mathcal{S}(\mathcal{T}_x) \otimes \mathcal{S}(\mathcal{T}_y)$ satisfying

$$\frac{2\Delta t}{3d_\alpha}\int_0^{\mathcal{Y}} y^{1-\alpha}\left(\nabla_{xy}\mathcal{U}_h^{n+1}(t), \nabla_{xy}\mathcal{V}_h\right)_{L^2(\Omega)} dy + \left(\operatorname{tr}\mathcal{U}_h^{n+1}, \operatorname{tr}\mathcal{V}_h\right)_{L^2(\Omega)}$$

$$= \left(\frac{4}{3}\operatorname{tr}\mathcal{U}_h^n - \frac{1}{3}\operatorname{tr}\mathcal{U}_h^{n-1}, \operatorname{tr}\mathcal{V}_h\right)_{L^2(\Omega)} + \frac{2\Delta t}{3}\left(f(\operatorname{tr}\mathcal{U}^n) - f(\operatorname{tr}\mathcal{U}^{n-1}), \operatorname{tr}\mathcal{V}_h\right)_{L^2(\Omega)}.$$

for all test functions $\mathcal{V}_h \in \mathcal{S}(\mathcal{T}_x) \otimes \mathcal{S}(\mathcal{T}_y)$. Note that the nonlinearity is treated explicitly. Since we expect this contribution to be non-stiff this should not cause concern. The fact that we

replaced the infinite cylinder $\Omega \times \mathbb{R}_+$ with $\Omega \times (0, \mathcal{Y})$ can be justified by the fact that when expanding $\mathcal{U}$ in an eigenbasis of the Laplacian, all contributions (except for the constant one) decay exponentially. (See [4, 24] for details in the Dirichlet case, the Neumann case behaves analogously). The cutoff of the constant contribution does not impact the result since we used homogeneous Neumann conditions on the artificial boundary, which capture the constant mode exactly. When referencing this algorithm, we will refer to it as the "hp-method".

In order to be able to compare the results obtained by our hp-FEM type approach, we also implemented and ran our experiments using a simpler spectral type method proposed in [5]. It directly exploits the spectral definition of the fractional Laplacian by using a discrete cosine transform. For time discretization we use an IMEX-type Euler method. When referencing this algorithm, we will refer to it as the "spectral–method".

3.1 Detecting an interface and measuring speeds

In order to extract information on the behavior of the interfaces, we need to fix our methodology for extracting the quantities of interest from the numerical solutions. For simplicity, even when using a high order method for solving (1) numerically, our measurements are always taken from a piecewise linear approximation to the numerical solution. This is done by interpolation on a finer grid.

Since the interfaces need a certain time to form, and we expect the interfaces to collapse after some time, with the scales of these timings depending on ε and α, we use an (empirically determined) estimate for the time until the collapse happens t_{col}, i.e., the solution becomes equal to the constant 1 function. When measuring we then assume that for $\frac{1}{4}t_{col}$ the interface has already formed and assume that afterwards, the interfaces remained stable for a duration of $\frac{1}{10}t_{col}$ and we can do accurate measurements.

When computing the speed of the interface, we consider the speed of the zeros of the numerical solution. In order to determine the width of the interface, we made the very simplistic assumption that an interface happens whenever the solution dips between $\max(u) - \delta$ and $\min(u) + \delta$. For the images chosen here we used $\delta := 0.1$. This gave good correspondence of the wave speed determined by the zeros of u and the speed of the midpoint of the interface. We also tested using $\delta = 0.01$ and $\delta \approx \varepsilon^\alpha$, but $\delta = 0.1$ seemed to give the most robust results. Both width and speed are computed by taking the average over 100 measurements in the time-frame $\left(\frac{1}{4}t_{col}, \frac{7}{20}t_{col}\right)$. Figure 2 shows a typical situation.

In order to determine rates, we used MATLABs *Curve Fitting Toolbox* for polynomial and power-law fits.

3.2 Model problem

For our computations we fixed the following parameters. We considered the domain $\Omega := (-L, L)$ with $L := 10$. In order to derive a starting condition which is close to the theoretical considerations of Section 2, we approximately computed a layer solution v, as described in Section A.1. Tacitly extending the function v by a constant outside of $(-L, L)$, the initial condition is then given by

$$u_0(x) := v\left(\frac{x - x_0}{\varepsilon}\right) + v\left(\frac{-x - x_0}{\varepsilon}\right) + 1.$$
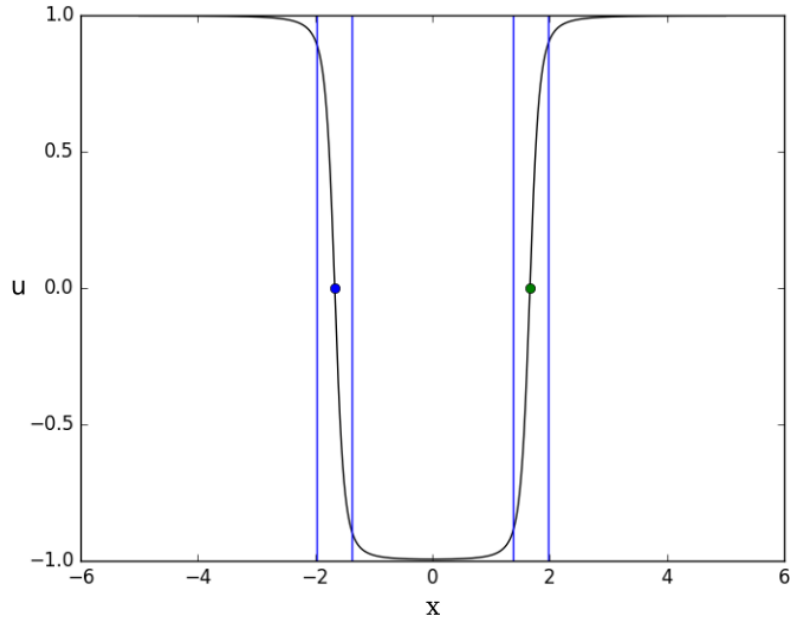
Figure 2: Example for the detected interfaces and roots.

This function possesses two interfaces at $\pm x_0$, which was taken to be $x_0 := L/4$. We will later on also discuss what happens for more general initial conditions. We used a timestepping size of $\Delta t := \min(0.05, 10^{-4} t_{col})$, ensuring that we make at least 10^4 steps.

For the spectral method we used a grid with $N = 262144$ points. For the hp-method, in Ω, we used a uniform grid of mesh size $\min(2L/\varepsilon, 8012)$ and polynomial degree $p_x = 5$ in order to resolve the appearing steep flanks of the interfaces well. To discretize the artificial variable, we used $p_y = 8$ on a geometric grid with 8 layers and a mesh grading factor of $\sigma = 0.125$, i.e., the grid consists of points of the form $8(0.125)^\ell$ for $\ell = 0, \ldots 8$.

3.3   Comparison of the two methods

In this section, we compare the different methods we used. Since they are quite different (first order vs second order in time, different approaches to the fractional Laplacian), we expect that this comparison gives a good indication of the real accuracy of our simulations. Instead of comparing the discrete solutions directly, we compare the postprocessed quantities: interface speed, interface width and time–to–collapse. The results are collected in Figure 3. As we can see, the error is reasonably small for all contributions, giving confidence that the behavior observed numerically matches the one of the exact solution. The only exception is for small values of $\alpha \approx 0.2$. As we do not expect our discretization to be robust as $\alpha \to 0$ this has to be expected. At the same time, this behavior may explain the observed mismatch between our predicted behavior and the observations in this regime.

4 Results on Metastability

In this section, we consider the evolution of two interfaces. We present the results of our numerical experiments on intervals $[-L, L]$ and compare them with our analysis on the real line. Therefore, it is natural to investigate the dependence of our quantities of interest on the size of the considered interval $[-L, L]$. As can be seen in Figure 4, neither the (modified) speed nor the width of the interface seem to depend strongly on the size of the domain. Especially for larger domains, the results become indistinguishable.

We illustrate the metastable behavior for solutions of the Allen-Cahn equation (1) with well–prepared initial data (11) with $L = 10$, $\varepsilon = 0.01$ and $\alpha = 0.9$ in Figure 5. In this simulation, we can define a time–to–collision $\widetilde{T}_C$ as the first time that two interfaces collide, i.e. $\widetilde{T}_C$ is the time at which the solution becomes non-negative. This happens at some time between $t = 3671.53$ and $t = 3694.24$, see Figure 5. We studied the evolution of interfaces also via the ODE system (14) which governs the evolution of the centers of interfaces. There the time–to–collision T_C is defined as the first time that two centers collide, see (16). Using the parameters of our simulation, T_C as given in (20) is approximately 3587.10, where we used $d_0 = 2$ as in the simulation and computed $\gamma = 1.28550$ as in Appendix A.1. Comparing $\widetilde{T}_C$ with T_C shows that the collision of interfaces takes place at a little later than expected.

Next, we will first discuss the interface speed $s = s(\varepsilon, \alpha)$ and, then, the interface width $w = w(\varepsilon, \alpha)$.

4.1 Interface speed $s = s(\varepsilon, \alpha)$

Due to the analysis of the evolution of interfaces of (1) on the real line, the (centers of) interfaces move according to the ODE system (14). In the case of two interfaces with centers x_1 and x_2, the interface speed satisfies approximately

$$
\begin{aligned}
s_{\mathbb{R}}(\varepsilon, \alpha) &\approx \left| \frac{\varepsilon^{1+\alpha}}{\alpha} 4 \frac{2^\alpha \Gamma((1+\alpha)/2)}{\sqrt{\pi}|\Gamma(-\alpha/2)|} \gamma \frac{x_1 - x_2}{|x_1 - x_2|^{1+\alpha}} \right| \\
&= \varepsilon^{1+\alpha} \frac{4}{\alpha} \frac{2^\alpha \Gamma((1+\alpha)/2)}{\sqrt{\pi}|\Gamma(-\alpha/2)|} \gamma \frac{1}{|x_1 - x_2|^\alpha} .
\end{aligned}
\tag{25}
$$

where $\gamma := (\int_{\mathbb{R}} (v'(x))^2 \mathrm{d}x)^{-1}$ and v is a basic layer solution of (9) satisfying $\lim_{x \pm \infty} v(x) = \pm 1$ and $v(0) = 0$.

In order to cross-validate this analysis, we measured the speed numerically. Renormalizing according to our previous considerations, we compute a renormalized speed

$$
\widehat{s}(\varepsilon, \alpha) := \frac{C_\alpha |x_1 - x_2|^\alpha}{\varepsilon^{1+\alpha}} s(\varepsilon, \alpha).
$$

with the normalization factor

$$
C_\alpha := \left(\frac{4}{\alpha} \frac{2^\alpha \Gamma((1+\alpha)/2)}{\sqrt{\pi}|\Gamma(-\alpha/2)|} \right)^{-1} = \frac{\Gamma(1-\alpha)}{2 \sec(\alpha \frac{\pi}{2})} .
$$

If the relationship (25) holds true, we expect that the renormalized speed then behaves like the factor γ. In Figure 6, we have plotted the relationship $\alpha \mapsto \widehat{s}(\varepsilon, \alpha)$ for different values

of ε. We first note, that all the curves (roughly) correspond to each other which hints that the ε–dependence is properly captured by the asymptotics. Comparing the resulting curve to the numerically computed value of γ then confirms the overall relationship.

4.2 Time–to–collapse t_{col}

The previous computation of the interface speed still relied on locating the interface and measuring its speed using a number of sample points. This might cause some hard to account for inaccuracies, resulting in small discrepancies to the predicted behavior and the slightly noisy look of Figure 6. In order to arrive at a second, more robust result, we also looked at the time it takes for the interfaces to collide and finally annihilate, what we call the *time–to–collapse t_{col}* for solutions of PDE (1). We compute it by comparing our numerical solution to the constant function taking the value 1 everywhere. If the difference, as measured in the L^2-norm, drops below 10^{-6} we record the current time and plot the analog to Figure 6.

The time–to–collapse t_{col} for solutions of the Allen-Cahn equation (1) with well–prepared initial data (11) is approximately/greater than the time–to–collision T_C in the associated ODE system (14) (up to some additive terms, see Theorems 2.3 and 2.5):

$$t_{col}(\varepsilon, \alpha) \geq \left(\frac{d_0}{\varepsilon}\right)^{1+\alpha} \frac{C_\alpha}{2(1+\alpha)\gamma}. \tag{26}$$

Computing the modified time–to–collapse as

$$\widehat{t}_{col} := \left(\frac{\varepsilon}{d_0}\right)^{1+\alpha} \frac{2(1+\alpha)}{C_\alpha} t_{col},$$

we expect that $\widehat{t}_{col} \geq \gamma^{-1}$ but to be of comparable size. Figure 7 confirms the estimate on $\widehat{t}_{col}$.

4.3 Interface width $w = w(\varepsilon, \alpha)$

Next, we consider the width of individual interfaces. For each fixed α, we can plot the interface width as a function of ε in a log-log plot as shown in Figure 8.

We see that the behavior with respect to ε can be approximated well by a power law of the form $w(\varepsilon, \alpha) \approx \varepsilon^{a(\alpha)} b(\alpha)$. In the second subplot of Figure 8, we plotted the behavior of the coefficient $a(\alpha)$ when varying α in $(0.2, 2)$. Namely, we chose a uniform grid of 40 points between 0.2 and 1.9. We see that the behavior especially in the regime of larger α, can be well modeled by $a(\alpha) \approx \kappa_1 \alpha^{-1} + \kappa_2$. Empirically we determined the constants in the fit as $\kappa_1 := -0.168298$ and $\kappa_2 := 1.11709$. Overall we see the empirical law

$$w(\varepsilon, \alpha) \approx b(\alpha) \varepsilon^{-0.168298\alpha^{-1} + 1.11709},$$

which is included in Figure 8 as the dotted black line. In order to get an estimate on $b(\alpha)$, we again rescale w to get

$$\widehat{w}(\varepsilon, \alpha) := w(\varepsilon, \alpha) \varepsilon^{0.168298\alpha^{-1} - 1.11709}. \tag{27}$$

We plot the behavior of $\widehat{w}$ in Figure 9. We observe that, while the ε-dependence is well captured for larger values of α, the behavior for small α is more erratic.

5 Summary and Outlook

Following the analysis of a fractional Allen-Cahn equation on $\mathbb{R}$, we obtained formulas for the interface speed and time–to–collision and its dependence on ε and α. In Section 4 we checked the validity of these formulas for our model on a bounded interval with homogeneous Neumann boundary conditions. Moreover, we studied numerically the behavior of the interface width well before the two interfaces collide. Following the analysis by Patrizi and Valdinoci, we considered *well–prepared initial data*, i.e., we started close to a metastable profile. Hence, we are now in the position to provide a good dynamical unterstanding of the fractional Allen-Cahn equation in its metastable regime. Yet, for the classical Allen-Cahn equation, it is well-known that there are four possible stages in the generation, propagation and annihilation of metastable patterns [10]: Starting from a large class of oscillating initial data, there is phase separation, then the formation of a metastable pattern, next a slow motion of the metastable pattern and (a possible) annihilation of two interfaces. The latter stages may repeat until either a constant stable state or a single basic layer solution remains. Thus, we are still missing a more detailed analysis of the early stages of the generation of metastable patterns for the fractional Allen-Cahn equation, which remains a topic for future work.

Another natural question is to try to extend the approach in [9] to the case of a fractional Allen-Cahn equation, i.e., to re-consider the auxiliary BVP (5) as a problem in its own right. We may ask what happens if we replace the second-order derivative by the fractional Laplacian? Is this problem still somehow connected to metastability? Is the solution unique if we require positivity in the interior? If so, what is its shape? If it has a peak near zero, what is the scaling of the spike layer as a function of ℓ, ε and α? These questions all remain to be dealt with in future work.

Another important direction is to consider other potentials F. In this work we considered a balanced potential, i.e. $F(-1) = F(1)$. To fully characterize the dynamics of the fractional Allen-Cahn equation for general unbalanced potentials is an open question, but see [25, §5] and [2, 7] as examples for encouraging results towards this goal.

A Dependence on the size of the domain

Since all our analytical insights are dependent on working on the full space $\mathbb{R}$, whereas our numerics is restricted to a finite interval, it is natural to investigate the dependence of our quantities of interest on the size of the considered interval $(-L, L)$. As can be seen in Figure 4, neither the (modified) speed nor the width of the interface seems to depend strongly on the size of the domain. Especially for larger domains, the results become indistinguishable.

A.1 Basic layer solution on $\mathbb{R}$

The layer solutions of (9)–(10) are – in fact – the stationary traveling wave solutions of (1), which are unique up to translations (see [7]) and locally asymptotically stable, see [2, 23]. Therefore we aim to approximate the layer solution as the stationary solution of (1). We use again the numerical scheme on intervals $[-L, L]$ as presented in Section 3. Starting our numerical scheme in Section 3 with $\varepsilon = 1$ and an initial datum u_0 given as the linear function connecting -1 and 1, we let the simulation run until a stationary state is reached. Finally we

compute

$$\int_{-\infty}^{\infty}|v'|^2\mathrm{d}x = \int_{-\infty}^{-L}|v'|^2\mathrm{d}x + \int_{-L}^{L}|v'|^2\mathrm{d}x + \int_{L}^{\infty}|v'|^2\mathrm{d}x\,.$$

The term $\int_{-L}^{L}|v'|^2\mathrm{d}x$ is computed from our numerical solution. Whereas for the first and third summand we use that the layer solution is an odd function (see [7, Thm. 2.4] and its tail behaves as

$$v(x) \approx 1 + px^{-\alpha} \quad \text{for } x \gg L \quad \text{where } p = -\frac{\sec(\alpha\pi/2)}{2\Gamma(1-\alpha)}\,,$$

see [25, Eq. (23)] and [7, Thm. 2.7]. Thus,

$$\begin{aligned}
\int_{-\infty}^{-L}|v'|^2\mathrm{d}x &= \int_{L}^{\infty}|v'|^2\mathrm{d}x \\
&= \int_{L}^{\infty}p^2\alpha^2 x^{-2\alpha-2}\mathrm{d}x \\
&= p^2\alpha^2\frac{-1}{2\alpha+1}x^{-2\alpha-1}\Big|_{L}^{\infty} \\
&= p^2\alpha^2\frac{1}{2\alpha+1}L^{-2\alpha-1}\,.
\end{aligned}$$

Summing up, we deduce

$$\int_{-\infty}^{\infty}|v'|^2\mathrm{d}x = \int_{-L}^{L}|v'|^2\mathrm{d}x + 2p^2\alpha^2\frac{1}{2\alpha+1}L^{-2\alpha-1}\,.$$

We again chose different values of L in order to investigate the influence of the choice of bounded domain, but observe that for larger intervals, the influence of the cutoff becomes negligible.

References

[1] F. Achleitner and C. Kuehn. Analysis and numerics of travelling waves for asymmetric fractional reaction-diffusion equations. *Comm. Appl. Ind. Math.*, 6(2):1–25, 2015.

[2] Franz Achleitner and Christian Kuehn. Traveling waves for a bistable equation with nonlocal diffusion. *Adv. Differential Equations*, 20(9-10):887–936, 2015.

[3] S. S. Alzahrani and A. Q. M. Khaliq. Fourier spectral exponential time differencing methods for multi-dimensional space-fractional reaction-diffusion equations. *J. Comput. Appl. Math.*, 361:157–175, 2019.

[4] Lehel Banjai, Jens M. Melenk, Ricardo H. Nochetto, Enrique Otárola, Abner J. Salgado, and Christoph Schwab. Tensor FEM for spectral fractional diffusion. *Found. Comput. Math.*, 19(4):901–962, 2019.

[5] Alfonso Bueno-Orovio, David Kay, and Kevin Burrage. Fourier spectral methods for fractional-in-space reaction-diffusion equations. *BIT*, 54(4):937–954, 2014.

[6] Kevin Burrage, Nicholas Hale, and David Kay. An efficient implicit FEM scheme for fractional-in-space reaction-diffusion equations. *SIAM J. Sci. Comput.*, 34(4):A2145–A2172, 2012.

[7] Xavier Cabré and Yannick Sire. Nonlinear equations for fractional Laplacians II: Existence, uniqueness, and qualitative properties of solutions. *Trans. Amer. Math. Soc.*, 367(2):911–941, 2015.

[8] Luis Caffarelli and Luis Silvestre. An extension problem related to the fractional Laplacian. *Comm. Partial Differential Equations*, 32(7-9):1245–1260, 2007.

[9] J. Carr and R. L. Pego. Metastable patterns in solutions of $u_t = \epsilon^2 u_{xx} - f(u)$. *Comm. Pure Appl. Math.*, 42(5):523–576, 1989.

[10] Xinfu Chen. Generation, propagation, and annihilation of metastable patterns. *J. Differential Equations*, 206(2):399–437, 2004.

[11] Serena Dipierro, Alessio Figalli, and Enrico Valdinoci. Strongly nonlocal dislocation dynamics in crystals. *Comm. Partial Differential Equations*, 39(12):2351–2387, 2014.

[12] Serena Dipierro, Giampiero Palatucci, and Enrico Valdinoci. Dislocation dynamics in crystals: a macroscopic theory in a fractional Laplace setting. *Comm. Math. Phys.*, 333(2):1061–1105, 2015.

[13] Serena Dipierro, Xavier Ros-Oton, and Enrico Valdinoci. Nonlocal problems with Neumann boundary conditions. *Rev. Mat. Iberoam.*, 33(2):377–416, 2017.

[14] María del Mar González and Regis Monneau. Slow motion of particle systems as a limit of a reaction-diffusion equation with half-Laplacian in dimension one. *Discrete Contin. Dyn. Syst.*, 32(4):1255–1286, 2012.

[15] Gerd Grubb. Regularity of spectral fractional Dirichlet and Neumann problems. *Math. Nachr.*, 289(7):831–844, 2016.

[16] Dongdong He, Kejia Pan, and Hongling Hu. A spatial fourth-order maximum principle preserving operator splitting scheme for the multi-dimensional fractional Allen-Cahn equation. *Appl. Numer. Math.*, 151:44–63, 2020.

[17] Tianliang Hou, Tao Tang, and Jiang Yang. Numerical analysis of fully discretized Crank-Nicolson scheme for fractional-in-space Allen-Cahn equations. *J. Sci. Comput.*, 72(3):1214–1231, 2017.

[18] Christian Kuehn. *Multiple time scale dynamics*, volume 191 of *Applied Mathematical Sciences*. Springer, Cham, 2015.

[19] Mateusz Kwaśnicki. Ten equivalent definitions of the fractional Laplace operator. *Fract. Calc. Appl. Anal.*, 20(1):7–51, 2017.

[20] Seunggyu Lee and Dongsun Lee. The fractional allencahn equation with the sextic potential. *Applied Mathematics and Computation*, 351:176 – 192, 2019.

[21] Anna Lischke, Guofei Pang, Mamikon Gulian, Fangying Song, Christian Glusa, Xiaoning Zheng, Zhiping Mao, Wei Cai, Mark M. Meerschaert, Mark Ainsworth, and et al. What is the fractional Laplacian? A comparative review with new results. *J. Comput. Phys.*, 404:109009, 2020.

[22] Huan Liu, Aijie Cheng, and Hong Wang. A fast Galerkin finite element method for a space-time fractional Allen-Cahn equation. *J. Comput. Appl. Math.*, 368:112482, 18, 2020.

[23] Luyi Ma, Hong-Tao Niu, and Zhi-Cheng Wang. Global asymptotic stability of traveling waves to the Allen-Cahn equation with a fractional Laplacian. *Commun. Pure Appl. Anal.*, 18(5):2457–2472, 2019.

[24] Jens Markus Melenk and Alexander Rieder. hp-FEM for the fractional heat equation. *IMA Journal of Numerical Analysis*, 04 2020. drz054.

[25] Y. Nec, A. A. Nepomnyashchy, and A. A. Golovin. Front-type solutions of fractional Allen-Cahn equation. *Phys. D*, 237(24):3237–3251, 2008.

[26] Ricardo H. Nochetto, Enrique Otárola, and Abner J. Salgado. A PDE approach to space-time fractional parabolic problems. *SIAM J. Numer. Anal.*, 54(2):848–873, 2016.

[27] Stefania Patrizi and Enrico Valdinoci. Crystal dislocations with different orientations and collisions. *Arch. Ration. Mech. Anal.*, 217(1):231–261, 2015.

[28] Stefania Patrizi and Enrico Valdinoci. Relaxation times for atom dislocations in crystals. *Calc. Var. Partial Differential Equations*, 55(3):Art. 71, 44, 2016.

[29] Stefania Patrizi and Enrico Valdinoci. Long-time behavior for crystal dislocation dynamics. *Math. Models Methods Appl. Sci.*, 27(12):2185–2228, 2017.

[30] Raffaella Servadei and Enrico Valdinoci. On the spectrum of two different fractional operators. *Proc. Roy. Soc. Edinburgh Sect. A*, 144(4):831–855, 2014.

[31] Alex Simmons, Qianqian Yang, and Timothy Moroney. A preconditioned numerical solver for stiff nonlinear reactiondiffusion equations with fractional laplacians that avoids dense matrices. *Journal of Computational Physics*, 287:254 – 268, 2015.

[32] Fangying Song, Chuanju Xu, and George Em Karniadakis. A fractional phase-field model for two-phase flows with tunable sharpness: algorithms and simulations. *Comput. Methods Appl. Mech. Engrg.*, 305:376–404, 2016.

[33] Pablo Raúl Stinga and José Luis Torrea. Extension problem and Harnack's inequality for some fractional operators. *Comm. Partial Differential Equations*, 35(11):2092–2122, 2010.

[34] Martin Stoll and Hamdullah Yücel. Symmetric interior penalty galerkin method for fractional-in-space allen-cahn equations, 2015.

[35] Fanhai Zeng, Fawang Liu, Changpin Li, Kevin Burrage, Ian Turner, and V. Anh. A Crank-Nicolson ADI spectral method for a two-dimensional Riesz space fractional nonlinear reaction-diffusion equation. *SIAM J. Numer. Anal.*, 52(6):2599–2622, 2014.

[36] Shuying Zhai, Zhifeng Weng, and Xinlong Feng. Fast explicit operator splitting method and time-step adaptivity for fractional non-local allencahn model. *Applied Mathematical Modelling*, 40(2):1315 – 1324, 2016.
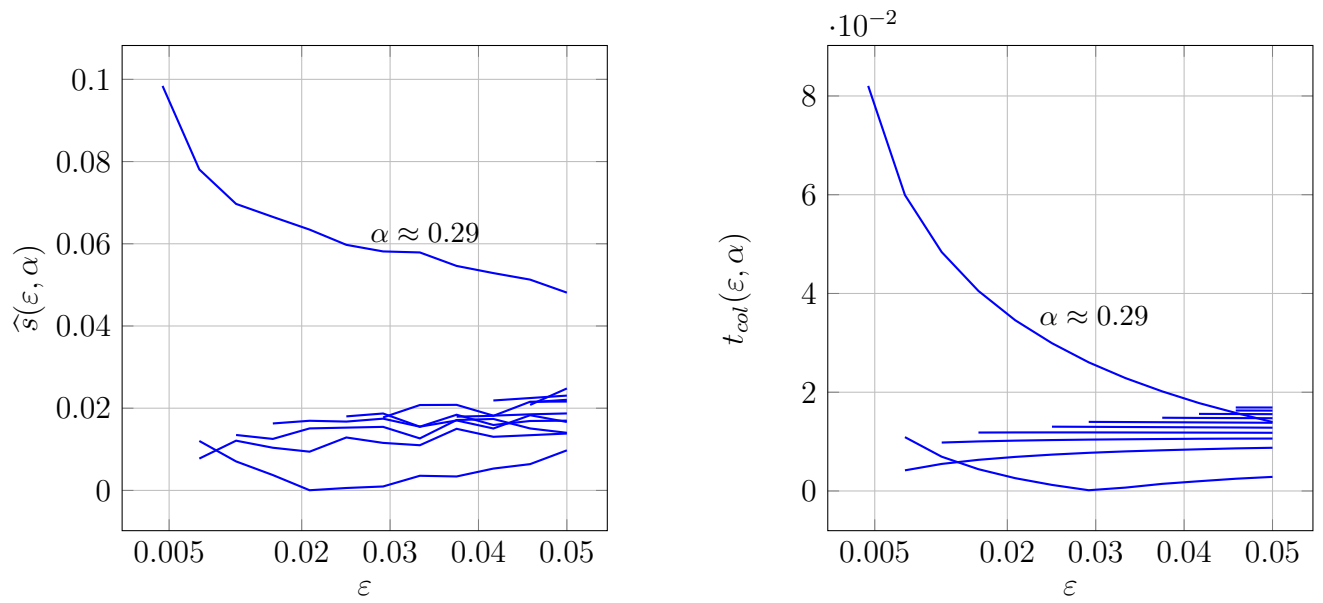
(a) Relative difference of the renormalized interface speed between the methods.

(b) Relative difference of the time–to–collapse between the methods.
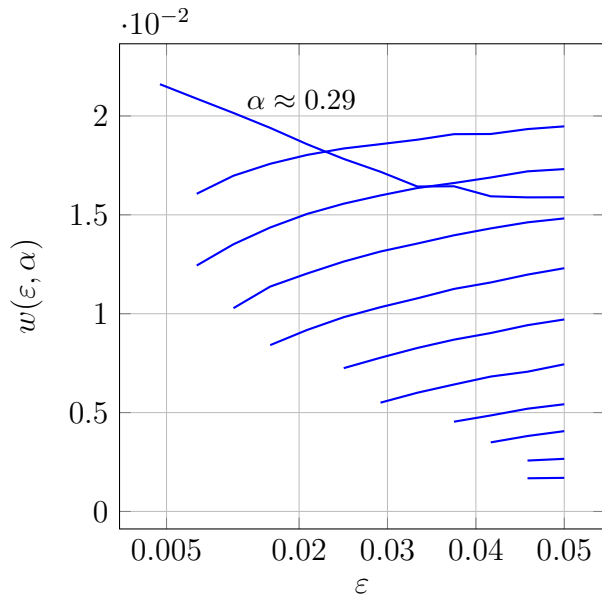
(c) Relative difference of the interface width between the methods.

Figure 3: Comparison of two numerical methods: hp–method vs. spectral–method. Different lines represent different values of $\alpha \in (0.2, 1.9)$.
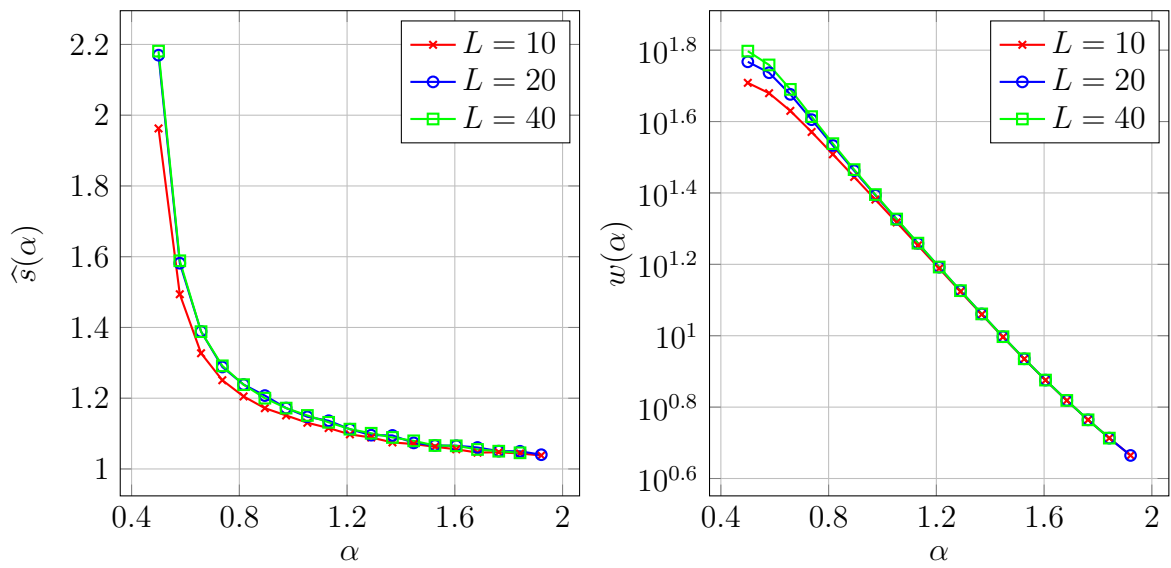
(a) Modified interface speed $\widehat{s}$.

(b) Interface width w.

Figure 4: Comparing results on intervals $[-L, L]$ with $L = 10, 20, 40$ and $\varepsilon = 0.1$.
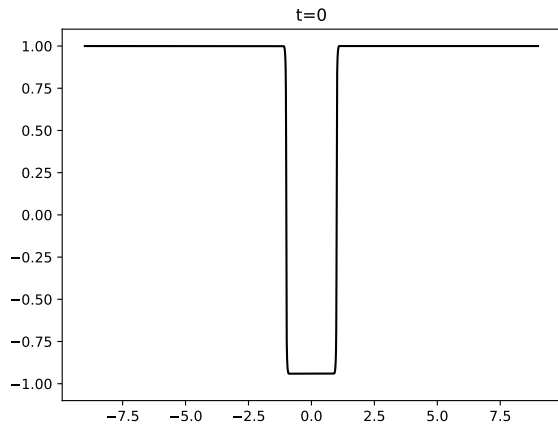
(a) solution at time $t = 0$.
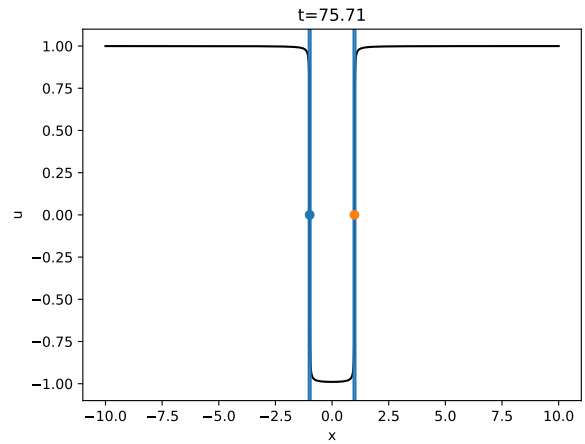
(b) solution at time $t = 75.71$.
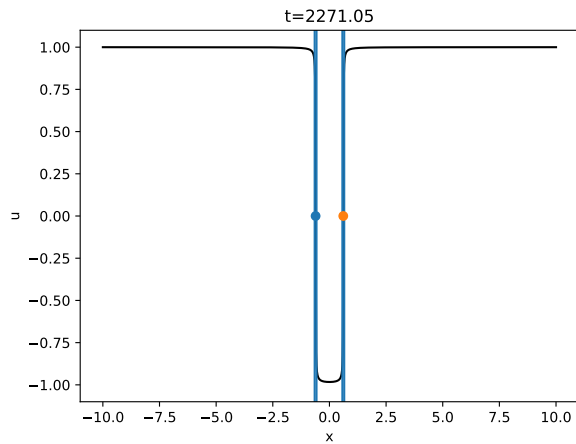
(c) solution at time $t = 2271.05$.
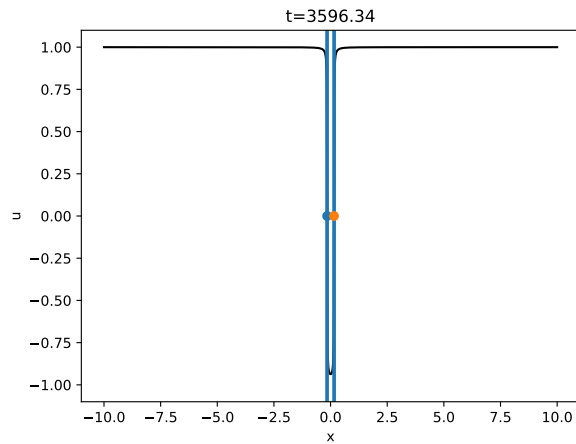
(d) solution at time $t = 3596.34$.
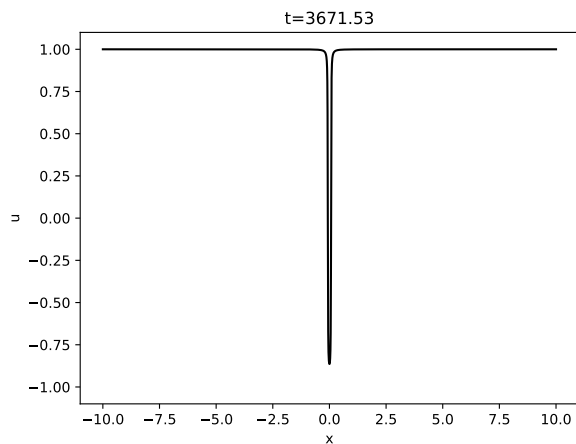
(e) solution at time $t = 3671.53$.
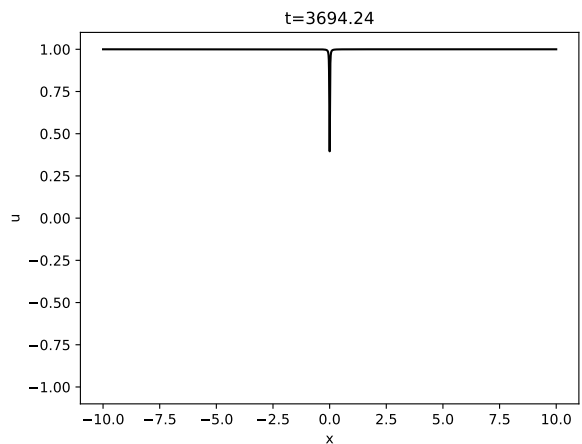
(f) solution at time $t = 3694.24$.

Figure 5: Evolution of solution for Allen-Cahn equation (1) with well–prepared initial data (11) with $L = 10$, $\varepsilon = 0.01$ and $\alpha = 0.9$.
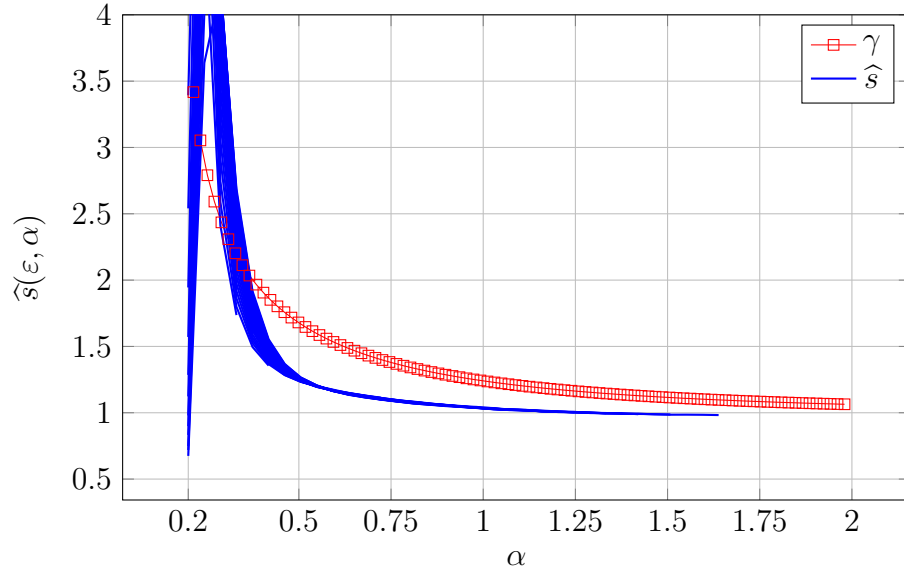
Figure 6: Comparison of the renormalized speed $\widehat{s}(\varepsilon, \alpha)$ to γ. Blue: different lines represent different values of $\varepsilon \in (0.002, 0.05)$.
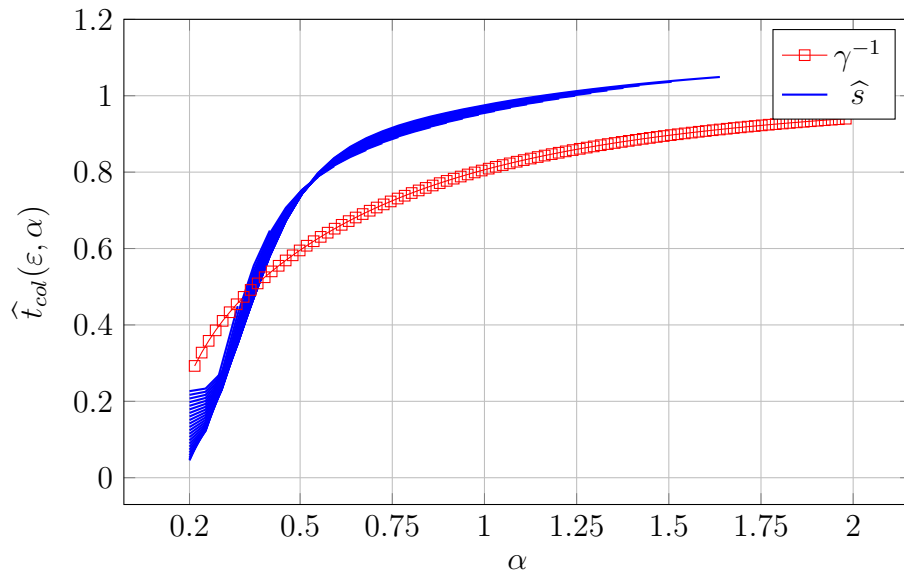
Figure 7: Comparison of the renormalized time–to–collapse $\widehat{t}_{col}$ to $1/\gamma$. Blue: different lines represent different values of $\varepsilon \in (0.002, 0.05)$.
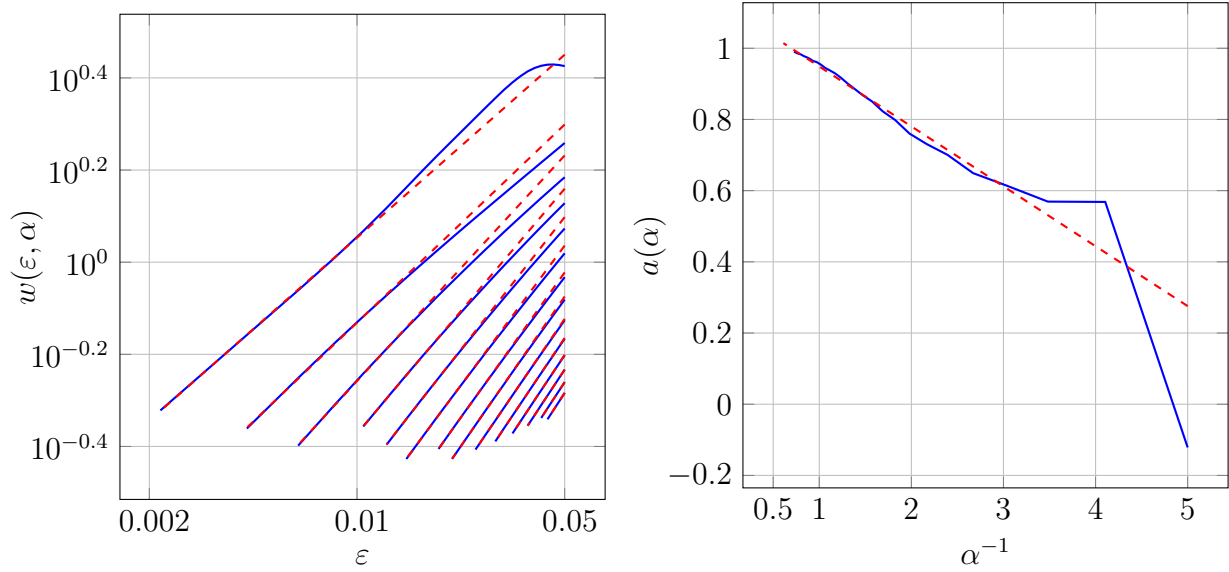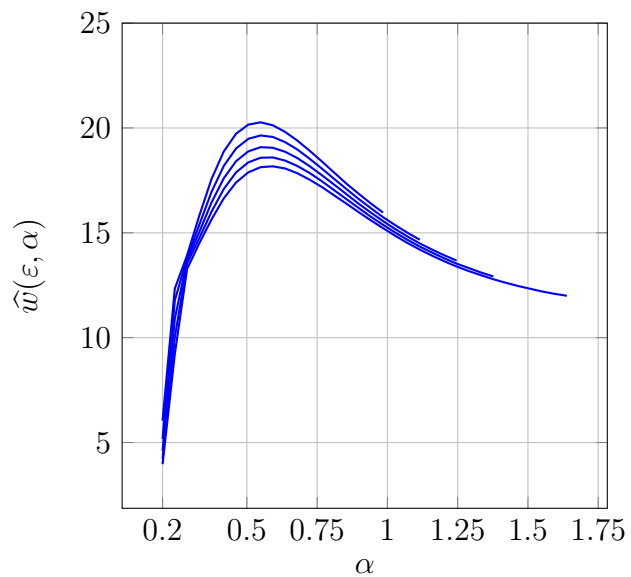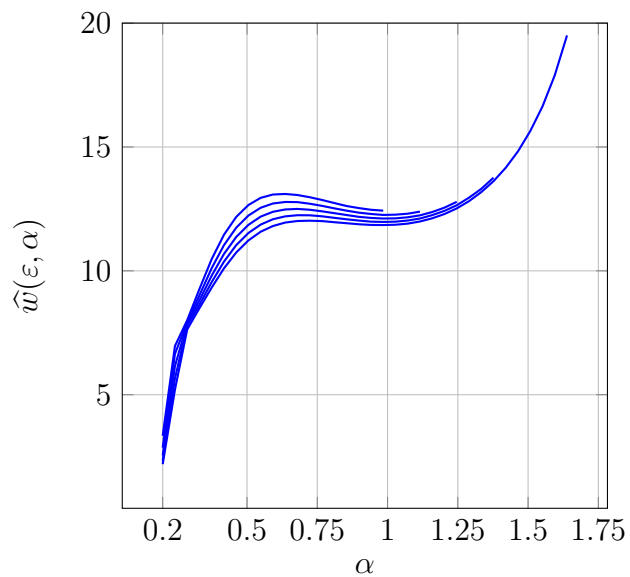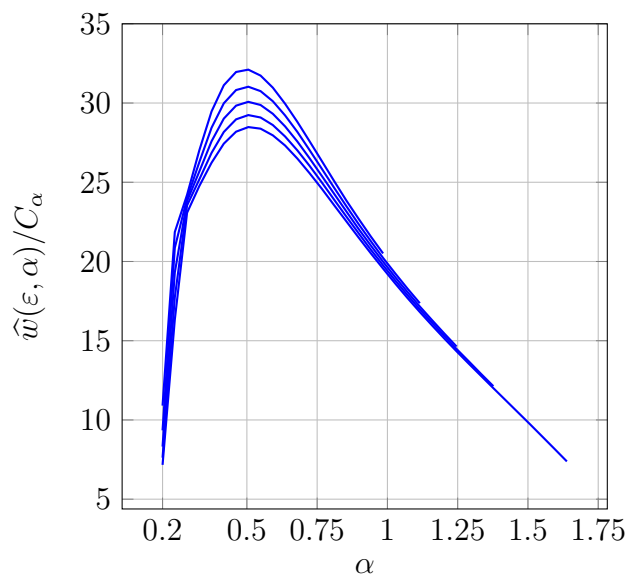
Figure 8: Behavior of the interface width (hp-BDF2 method). Different lines represent different values of α. Blue line: actual data; black dashed line: power law fit $w(\varepsilon, \alpha) \approx \varepsilon^{a(\alpha)} b(\alpha)$.

(a) Behavior of $\widehat{w}(\varepsilon, \alpha)$ in (27).

(b) Same as in (a), but also correcting using C_α.

(c) Same as in (a), but also correcting using C_α (alternative version).

Figure 9: Behavior of the modified interface width $\widehat{w}(\varepsilon, \alpha)$ with respect to α. Different lines represent different values of ε.
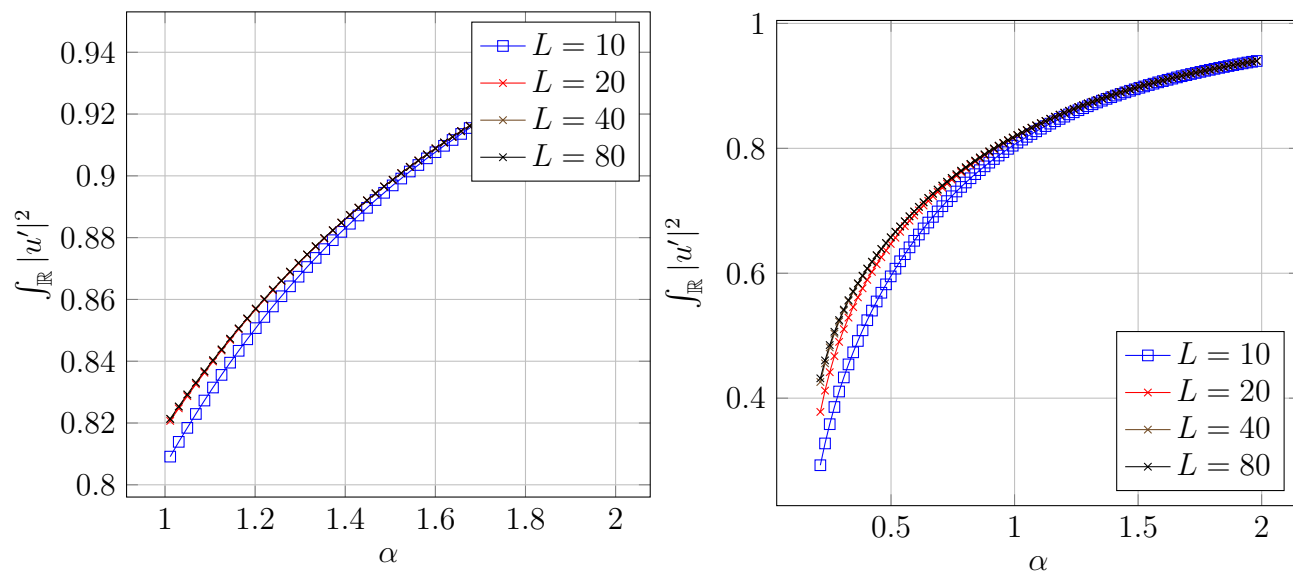
Figure 10: H^1-seminorm $\int_{-\infty}^{\infty} |v'|^2 \mathrm{d}x$ of a basic layer solution v of (9)–(10).